# The $ZrO_2$-$TiO_2$ phase diagram

ULRIKE TROITZSCH*, DAVID J. ELLIS
*The Australian National University,Department of Earth and Marine Sciences, Canberra ACT, 0200, Australia*
*E-mail: ulrike@ems.anu.edu.au*

The $ZrO_2$-$TiO_2$ phase diagram was determined experimentally between 800 and 1200°C, 1 atm, extending our knowledge of this system to temperatures previously inaccessible for equilibrium experiments due to sluggish kinetics. The crystallization of the ordered $(Zr,Ti)_2O_4$ phase from the oxides was facilitated by the addition of flux (CuO or $Li_2MoO_4/MoO_3$), and seeds. Two ordered $(Zr,Ti)_2O_4$ phases with different compositions were identified, and their phase relationships with $TiO_2$ and $ZrO_2$ solid solutions investigated. Structure data, superstructure reflections and composition were used to locate the ordering phase transition of $(Zr,Ti)_2O_4$ in equilibrium with $ZrO_2$ and $TiO_2$. At the onset of ordering between 1130 and 1080°C, $(Zr,Ti)_2O_4$ is of composition $X_{Ti} = 0.495 \pm 0.02$, and displays a dramatic change in b-dimension. At 1060°C and below, the composition of $(Zr,Ti)_2O_4$ is significantly more Ti-rich and dependent on temperature, ranging from $X_{Ti} = 0.576$ at 1060°C to 0.658 at 800°C. This variability in composition of the ordered phase contrasts with previous studies that suggested the composition to be constant at either $X_{Ti} = 0.667$ [$ZrTi_2O_6$] or 0.583 [$Zr_5Ti_7O_{24}$]. When grown at low temperatures and with lithium molybdate, the crystals of ordered $(Zr,Ti)_2O_4$ are acicular to needle shape, and develop distinct square cross-sections and end facets.


## 1. Introduction

The $ZrO_2$-$TiO_2$ phase diagram has been intensively studied over many years because it plays an important role for the synthesis and processing of industrial ceramics based on the various polymorphs of the compounds $TiO_2$, $ZrO_2$, and $(Zr,Ti)_2O_4$ [1–7]. Especially the intermediate phase zirconium titanate $(Zr,Ti)_2O_4$, which is a solid solution including compounds such as $ZrTiO_4$, $Zr_5Ti_7O_{24}$ and $ZrTi_2O_6$ (Srilankite), has received much attention in the past due to its outstanding dielectric properties in the microwave frequency range [8–12]. These properties make it a candidate for ceramic resonators in wireless communication apparatus such as GPS and mobile phones, a market sector that currently enjoys exponential growth. The accurate knowledge of the $ZrO_2$-$TiO_2$ phase diagram is essential for the design and production of high-quality ceramics based on these chemical compounds, especially when low-temperature synthesis methods are targeted.

While detailed phase diagrams are available for the high-temperature regions above 1200°C, [6, 7] where reactions proceed rapidly and synthesis experiments result in true equilibrium assemblages, such experiments are made difficult at lower temperatures due to slow kinetics. For example, experimental studies disagree significantly on the location of the two-phase field tetragonal-monoclinic $ZrO_2$ [1, 4, 5, 13] because heating and cooling experiments are characterized by hysteresis effects of up to 300 K [14, 15]. Another specific problem caused by slow kinetics in this system has been the crystallization of ordered $(Zr,Ti)_2O_4$, the stable intermediate phase below 1125°C, because it simply does not form spontaneously from the oxides in its stability field. This could be due to slow diffusion of the reactants, slow reaction rates, or nucleation problems. The difficulties of obtaining well-crystallized $(Zr,Ti)_2O_4$ at equilibrium below 1200°C "have frustrated attempts ... [to clarify] the stable low-temperature phase relations" [16].

Therefore, earlier studies synthesised the ordered phase exclusively via the disordered polymorph, which was sintered well above 1300°C and then cooled slowly, allowing the material to order successively between 1125 and 800°C [17]. With this synthesis method, the degree of order in the structure is significantly influenced by the cooling rate [11], and by additives such as $Y_2O_3$ [7]. While these experiments showed that an ordered $(Zr,Ti)_2O_4$ phase is stable at lower temperatures, the exact compositional boundaries of its stability field could not be determined because of the uncertain state of equilibrium of the samples that had been cooled slowly over hundreds of degrees. McHale and Roth [7] suggested the ordered phase to be of composition $X_{Ti} = 0.67$ [$ZrTi_2O_6$],

*Author to whom all correspondence should be addressed.
0022-2461 
DOI: 10.1007/s10853-005-1116-7

because they observed a tripled *a*-dimension compared to the disordered phase ($\alpha$-$PbO_2$ structure), indicative of a structure type $AB_2O_6$ such as fersmite. Sham *et al*. (1998) proposed $Zr_5Ti_7O_{24}$ to be the stable ordered phase, based on X-ray diffraction (XRD) patterns of samples prepared via the sol-gel method, and annealed at low temperatures [18]. The sol-gel method however, is prone to result in metastable phases in the $ZrO_2$-$TiO_2$ system, so that the equilibrium state of those samples is also uncertain [19, 20]. The composition of ordered $(Zr,Ti)_2O_4$ in equilibrium with other phases is not reported, possibly due to small grain size and $ZrO_2$-inclusions making microanalysis difficult.

From a manufacturing point of view, the synthesis method of ordered $(Zr,Ti)_2O_4$ by slow cooling below 1125°C has the disadvantage that cracks develop in the sample due to the volume change induced by the ordering transition [7]. Moreover, the ordering of $(Zr,Ti)_2O_4$ goes hand in hand with a change in composition towards higher Ti-contents, thus causing exsolution of a $ZrO_2$ phase which remains in the sample as impurity. Both $ZrO_2$ impurities and shrinkage cracks diminish the dielectric properties of the $(Zr,Ti)_2O_4$ ceramic, which is therefore rendered useless for industrial purposes and precise dielectric measurements [10]. Because of this synthesis difficulty, it is the disordered, high-temperature polymorph that is exclusively used in industry today, rather than the ordered form. Note that increasing order of the crystal structure has in fact been suggested to improve the dielectric properties of $(Zr,Ti)_2O_4$, but the experimental evidence was not conclusive due to lack of high-quality samples [10].

The recent development of a high-pressure synthesis method of the ordered phase directly from the oxides inspired the present study [21, 22]. This high-pressure method succeeded in the growth of the ordered phase from the oxides at equilibrium below 1125°C by addition of a flux. The study also found that the reaction does not occur spontaneously at pressures below 13 kbar, and that seeds of ordered $(Zr,Ti)_2O_4$ have to be added to overcome apparent nucleation difficulties of the ordered phase from the oxides. Thus, the present study is based on synthesis experiments at atmospheric pressure that were catalysed by a flux and seeds of ordered $(Zr,Ti)_2O_4$ obtained at high pressure. This new data helps refine the $ZrO_2$-$TiO_2$ phase diagram below 1200°C.

## 2. Experimental procedure

Experimental details are shown in Table I. Starting mixes were prepared from the oxides $TiO_2$ (Degussa), $ZrO_2$ (SPEX), CuO (Aldrich), $Li_2MoO_4$ (Aldrich), $MoO_3$ (Analar), and $(Zr,Ti)_2O_4$ seeds. The ordered phase with composition $X_{Ti} = 0.61$ used for seeding was synthesised from the oxides at 20 kbar and 1200°C with an ammonium carbonate mixture as flux, as described in Troitzsch *et al*. [20]. Fluxes used were either CuO, or a mixture of $Li_2MoO_4$ and $MoO_3$ in a mass ratio of 1:1.6 [28]. The oxides $ZrO_2$ and $TiO_2$ were

TABLE I Experimental run conditions and results used in Figs 2, 3 and 4. Run products are solid solutions of $ZrO_2$ [Z], $(Zr,Ti)_2O_4$ [ZT] and $TiO_2$ [R]. Phases that occur in trace amounts, or as relic phases which are not part of the equilibrium assemblage, are bracketed. Subscripts show composition of the phases [mol% $TiO_2$] determined with SEM. Standard deviation for all data points is less than 1 mol% (for R and Z) and 1.5 mol% (ZT below 1200°C), except when compositional ranges are given (e.g. $ZT_{63.3-69.2}$) based on maximum/minimum values. Also shown are the unit-cell dimension *b* of $(Zr,Ti)_2O_4$, and the relative intensity of superstructure reflection [200] compared to main peak [311] of $(Zr,Ti)_2O_4$, for those samples whose XRD pattern allowed their determination

| Run no. | Mix $TiO_2$ mol.% | Flux | Seeds | T [°C] | Time [h] | Run products[#] | *b* of ZT [Å] | Rel. Int. [200]% |
|---|---|---|---|---|---|---|---|---|
| 1/ATMU140 | 65 | LiMo | + | 800 | 168 | $Z_{2.8} + ZT_{64.0-65.8} + R_{99.7}$ | 5.320(1) | 20.2 ± 3.2 |
| 2/ATMU121 | 65 | CuO | + | 950 | 192 | $Z_{3.7} + ZT_{61.9-63.3} + R_{97.0}$ | 5.326(1) | 7.1 ± 0.6 |
| 3/ATMU108 | 35 | CuO | + | 1000 | 144 | $Z_{4.2} + ZT_{59.8}$ | 5.330(1) | 7.3 ± 0.9 |
| 4/ATMU109 | 70 | CuO | + | 1000 | 144 | $ZT_{62.5} + R_{96.4}$ | 5.328(1) | 7.3 ± 0.5 |
| 5/ATMU122 | 65 | CuO | + | 1020 | 168 | $ZT_{59.3-61.6} + R_{96.1}$ | 5.331(1) | 8.1 ± 0.4 |
| 6/ATMU117 | 35 | CuO | + | 1060 | 161 | $Z_{5.8} + ZT_{59.1-62.3} + (R_{95.3})$ | 5.344(1) | 7.3 ± 2.3 |
| 7/ATMU118 | 70 | CuO | + | 1060 | 161 | $(Z_{5.8}) + ZT_{58.1-61.6} + R_{94.4}$ | 5.344(1) | 5.5 ± 1.3 |
| 8/ATMU177 | 55 | LiMo | + | 1060 | 120 | $Z_{6.5} + ZT_{59.0} + R_{95.9}$ | 5.337(1) | – |
| 9/ATMU176 | 55 | LiMo | + | 1080 | 96 | $Z_{8.2} + ZT_{48.1-49.6}{}^{*} + R_{94.4}$ | 5.397(1) | – |
| 10/ATMU96 | 3 | CuO | – | 1100 | 93 | $Z_{3.0}$ | – | – |
| 11/ATMU96 | 7 | CuO | – | 1100 | 93 | $Z_{4.0} + Z_{9.8}$ | – | – |
| 12/ATMU96 | 11 | CuO | – | 1100 | 93 | $Z_{11.1}$ | – | – |
| 13/ATMU96 | 20 | CuO | – | 1100 | 141 | $Z_{13.7} + R_{94.6}$ | – | – |
| 14/ATMU113 | 35 | CuO | + | 1100 | 141 | $Z_{13.3} + ZT^{*} + (R_{94.0})$ | – | – |
| 15/ATMU114 | 70 | CuO | + | 1100 | 96 | $Z + ZT^{*} + R_{93.3}$ | – | – |
| 16/ATMU169 | 55 | LiMo | + | 1105 | 120 | $(Z) + ZT_{48.8-50.7}{}^{*} + R_{94.0}$ | 5.423(1) | – |
| 17/ATMU163 | 75 | CuO | + | 1110 | 168 | $Z_{13.7} + ZT_{51.6-52.0}{}^{*} + R_{94.4}$ | – | 2.3 ± 1.7 |
| 18/ATMU168 | 55 | LiMo | + | 1130 | 96 | $(Z) + ZT_{48.7-50.3}{}^{*} + R_{93.3}$ | 5.444(1) | – |
| 19/ATMU115 | 70 | CuO | + | 1160 | 96 | $ZT_{52.1} + R_{93.6}$ | 5.465(1) | – |
| 20/ATMU116 | 35 | CuO | + | 1160 | 96 | $Z_{13.0} + ZT_{50.9}$ | 5.465(1) | – |
| 21/ATMU73/5 | 50 | – | – | 1200 | 86 | $(Z) + ZT_{50.0} + (R)$ | 5.473(1) | – |
| 22/ATMU70/5 | 50 | – | – | 1400 | 25 | $ZT_{50.0}$ | 5.479(1) | – |
| 23/ATMU72/5 | 50 | – | – | 1600 | 31 | $ZT_{50.0}$ | 5.484(1) | – |

[#] All run products contain traces of the respective flux

*Composition of ZT that surrounds cores of composition $X_{Ti} = 0.61$ (ie. ZT-seeds).

dried at 1100°C before weighing into various proportions. About 5 wt.% of seeds and 5 wt.% of either flux were added to all samples to be equilibrated below 1200°C, and everything ground together with acetone in an agate mortar. About 20 to 40 mg of the starting mix was pressed into 2-mm platinum-capsules, which were crimped shut. The bench-top muffle furnace used for experiments has an accuracy of ±1°C. At the end of each run the samples were quenched to room temperature in less than one minute in order to prevent any further ordering of $(Zr,Ti)_2O_4$ during cooling.

Although both fluxes catalysed the formation of ordered $(Zr,Ti)_2O_4$, each flux slowly disappeared during the experiments, sometimes even before the reaction was complete. This is probably due to evaporation since both fluxes have a high volatility. In addition, copper slowly alloyed with the Pt-capsule.

In an attempt to grow large single crystals of ordered $(Zr,Ti)_2O_4$, one experiment (ATMU134) was carried out with an especially large amount of lithium molybdate flux (70 wt.%). This time the seeds were not ground with the mix, but added as one layer sandwiched between the $ZrO_2$-$TiO_2$-flux mix inside a 5-mm Platinum-capsule. The sample was equilibrated at 800°C for 96 hours, resulting in single crystals $(Zr,Ti)_2O_4$ up to 0.1 mm long (see below).

All samples except ATMU134 were analysed with a Siemens D501 diffractometer using Cu K$\alpha$ radiation, between 5 and 90° 2-theta, at a step width of 0.02° and scan speed of 0.5° per minute. Unit-cell dimensions of $(Zr,Ti)_2O_4$ were determined with the Rietveld method using the program RIETAN-2000 to facilitate the detection of order in the structure [7, 23]. Quantitative analyses were obtained with a JEOL JSM-6400 scanning electron microscope at 15 kV and 1 nA, using synthetic, homogenous zirconolite as standard for Zr and Ti.

## 3. Results and discussion

### 3.1. Equilibrium composition

Experimental results are listed in Table I, which reports what we interpret to represent the equilibrium composition of each phase, based on textural evidence and reproducibility of the composition across the sample [20, 21].

The equilibration of assemblages involving ordered $(Zr,Ti)_2O_4$ was commonly incomplete, and only experiments at 1000 and 1020°C resulted in two-phase assemblages that would be expected based on the Gibbs phase rule (Fig. 1a). These temperatures seem to promote reaction rates of the ordered phase that are fast enough to overcome the problem of flux evaporation discussed above. Those samples that only reached local equilibrium displayed reaction textures that helped to identify the actual equilibrium compositions of the phases. Examples are pure $ZrO_2$ relics that are fully enclosed in a more Ti-rich $ZrO_2$ solid solution of homogeneous composition, and cores of seed composition in ordered $(Zr,Ti)_2O_4$, that are surrounded by a distinct rim of different composition (Fig. 1d and e). In these cases the cores were regarded as relics, and the rim as the new equilibrium compositions. In contrast to this, $TiO_2$ solid solution generally equilibrated completely throughout the grains, suggesting that the diffusion rate or reactivity of Zr could be a major controlling factor in this system.

### 3.2. Fluxes

The CuO-melt flux, which it is known to perform well in high-P experiments, [20] produced well-equilibrated to partly-equilibrated assemblages (Fig. 1a+b, runs no. 2 to 7 in Table I) except below 950°C and between about 1080 and 1130°C (Table I). Experiments in these temperature regions were therefore carried out with lithium molybdate flux.

The ineffectiveness of CuO-flux below 950°C suggests that the melting point of the $ZrO_2$-$TiO_2$-CuO system is approached, and that samples below that temperature were sub-solidus, and thus without the diffusion-enhancing effect of the CuO-melt flux. Although the melting point of this ternary system is not precisely known, the onset of melting near 950°C would be consistent with the eutectic temperatures of the binary systems CuO-$ZrO_2$ and CuO-$TiO_2$ at 1130 and 910°C, respectively, with very Cu-rich eutectic compositions (>84 mol% CuO) [24,25]. Run No. 1 at 800°C (Table I) was therefore carried out with the lithium molybdate flux, which has a lower melting point than the CuO flux. Although three phases are present in this sample (solid solutions of rutile, zirconia and ordered $(Zr,Ti)_2O_4$) (Fig. 1c), indicating that it only equilibrated locally, all three phases have homogeneous compositions across the sample that are consistent with the experiments at higher temperature (Fig. 2). Ordered $(Zr,Ti)_2O_4$ developed into well-shaped, elongated crystals of homogeneous composition, which are much larger than the original seeds, thus clearly indicating growth of the phase from the oxides. While lithium molybdate flux worked better than CuO at this temperature, its volatility still caused it to evaporate before the reaction was complete.

The diminished effectiveness of the CuO flux above 1080°C could be due to increased reduction of $Cu^{2+}$ to $Cu^{+}$ [24], and/or faster evaporation of the copper oxide at these temperatures. The failure of the CuO flux at these temperatures is demonstrated for example by experiments 14 and 15 (Table I) in which $ZrO_2$ and $TiO_2$ solid solutions reached equilibrium, whereas the ordered phase was present only as the seeds that were part of the starting mix, and had not grown. The complete equilibration of the samples with CuO at 1160°C (runs 19 and 20, Table I) was possibly helped by the fact that it was disordered $(Zr,Ti)_2O_4$ that crystallized, which is known to react more rapidly compared to the ordered phase.

In contrast to CuO, the lithium molybdate flux catalysed the reactions in our experiments, in particular the growth of ordered $(Zr,Ti)_2O_4$, across the entire temperature range discussed here (800 to 1200°C). However, the samples equilibrated only locally, leaving behind abundant relic phases of the starting mix.

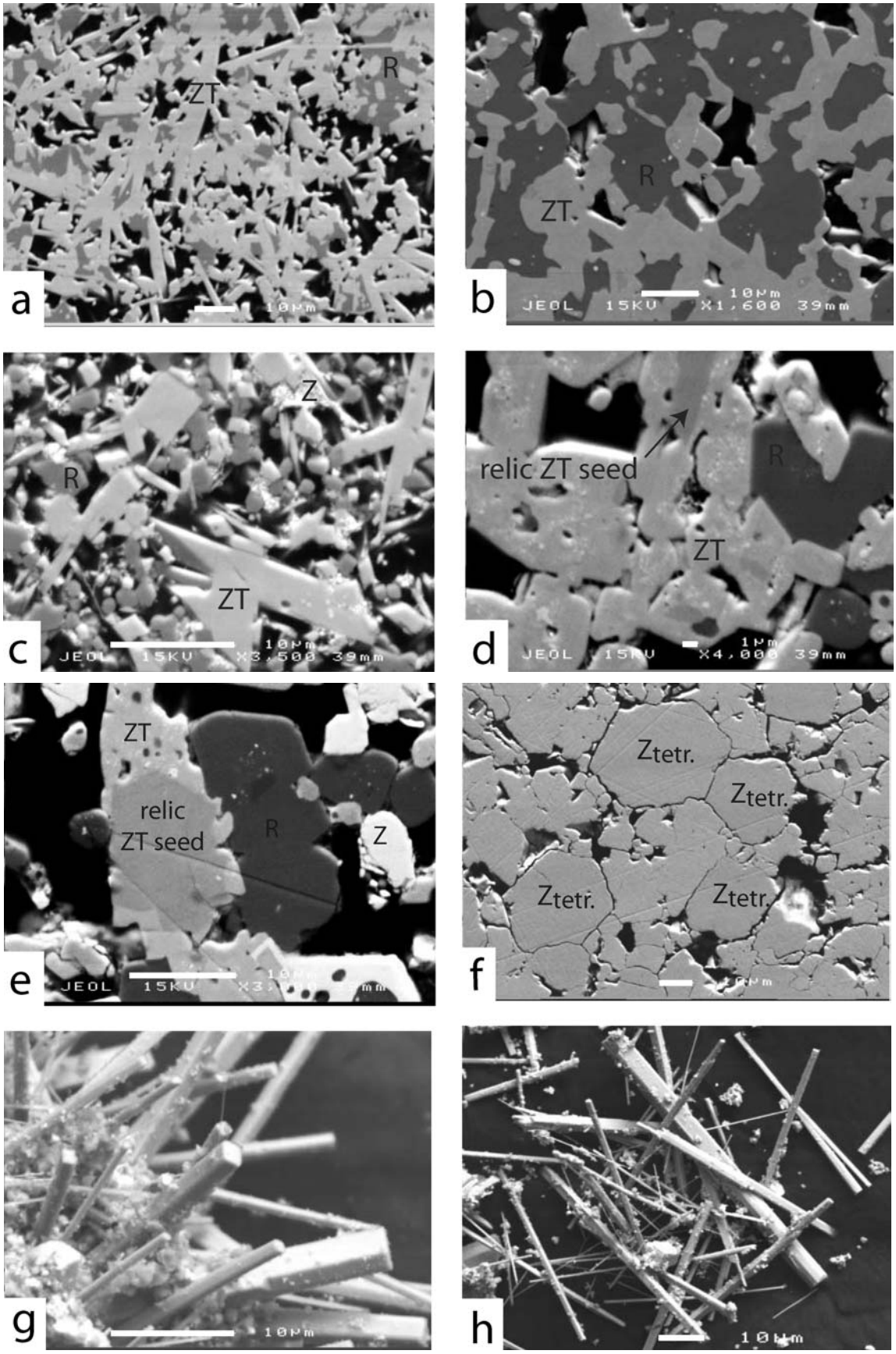


*Figure 1* SEM images of polished (a to f) and unpolished samples (g and h). (a) 4/ATMU109, (b) 19/ATMU115, (c) 1/ATMU140, (d) 18/ATMU168, (e) 9/ATMU176, (f) 10/ATMU96, (g) and (h) ATMU134. Scale bars are 1 $\mu$m in (d), and 10 $\mu$m in all others. Abbreviations: Z-zirconia, R-rutile, ZT-zirconium titanate, tetr.-tetragonal.

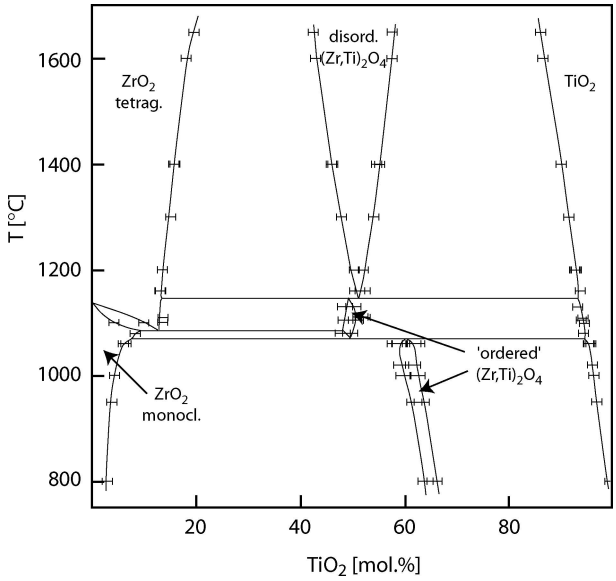


*Figure 2* The $ZrO_2$-$TiO_2$ phase diagram at atmospheric pressure based on experimental data (Table I). Data above 1200°C from Troitzsch and Ellis (2004) [21]. Note that all phases (tetragonal and monoclinic $ZrO_2$, ordered and disordered $(Zr,Ti)_2O_4$, $TiO_2$) are solid solutions, and the phase fields are labelled with the predominant end-member. No distinction is made between partly or fully ordered $(Zr,Ti)_2O_4$, and the label 'ordered' encompasses both in this study.

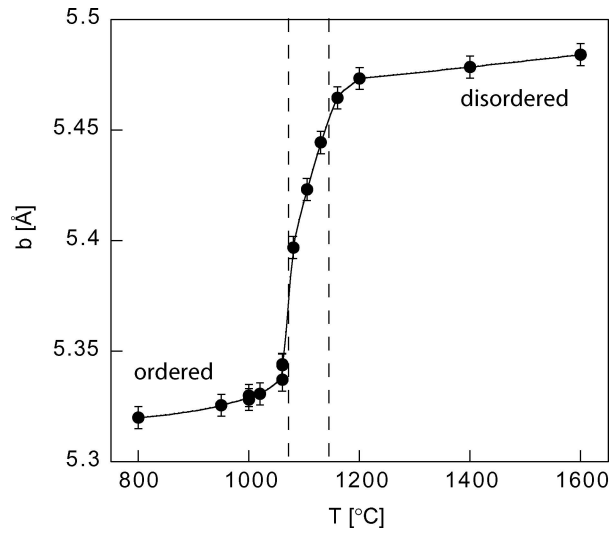


*Figure 3* Unit-cell dimension *b* of $(Zr,Ti)_2O_4$ at different temperatures (Table I). Dashed lines refer to the compositional jumps of the $(Zr,Ti)_2O_4$ phase as shown in the phase diagram (Fig. 2).

## 3.3. Order in the $(Zr,Ti)_2O_4$ structure

The *b*-dimension is a well-known, sensitive indicator for the state of ordering in $(Zr,Ti)_2O_4$, and was determined for every sample (Table I, Fig. 3). Note that previous studies reporting the change in *b* with temperature, used samples that were of constant composition (usually $X_{Ti} = 0.50$). These were also cooled slowly to the target temperature and then quenched [26,27]. In contrast to this, the data shown in Fig. 3 are based on the equilibrium composition of $(Zr,Ti)_2O_4$ at each temperature, thus applying directly to the phase diagram. Only above 1200°C, where the composition of the disordered phase spans up to 16 mol.% were samples with $X_{Ti} = 0.50$ used, which is close to the average composition (runs 21 to 23, Table I). Fig. 3 shows that

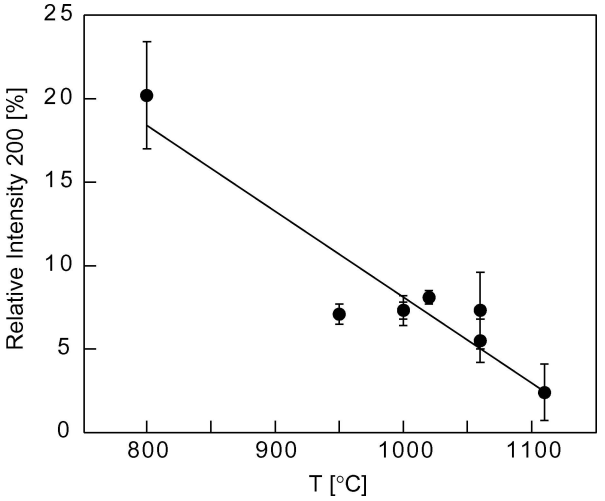


*Figure 4* Relative intensity of superstructure reflection [200] compared to main peak [311] of ordered $(Zr,Ti)_2O_4$ (Table I). Errors were based on absolute peak hight relative to background scatter.

equilibrium $(Zr,Ti)_2O_4$ begins to order somewhere below 1200°C,with a significant drop in *b*, between 1160 and 1060°C, indicating major rearrangement, i.e. ordering of the structure.

Another indicator of ordering is the appearance and intensity of superstructure reflection [200] in the XRD pattern of ordered $(Zr,Ti)_2O_4$. Fig. 4 shows how the intensity of the [200] peak relative to the main peak [311] (Table I) decreases with temperature. The linear extrapolation of this trend to zero intensity suggests that the onset of ordering lies near $1158 \pm 10$, which is in good agreement with the estimates based on the *b*-dimension (Fig. 3) and the compositional jump (Fig. 2). Note that the intensity at 1100°C (Fig. 4) may be may be slightly overestimated due to the presence of relic seeds of ordered $(Zr,Ti)_2O_4$ from the starting mix (Table I footnote). The appearance of the superstructure reflection in the XRD patterns (Table I) cannot be used as the sole measure for the onset of ordering, because the reflection is initially very weak and may be drowned in the background scatter, especially since ordered $(Zr,Ti)_2O_4$ comprises only a few percent in most of the samples equilibrated near the onset of ordering (runs 9 to 18).

Due to lack of TEM data of the samples presented here it is not possible to distinguish between a partly or fully ordered structure. The term 'ordered' as used throughout this study thus refers to both partly and fully ordered $(Zr,Ti)_2O_4$, without discerning exact ordering patterns [17, 29].

## 3.4. Phase diagram

Fig. 2 shows the $ZrO_2$-$TiO_2$ phase diagram constructed from the experimental data presented here (Table I), combined with those of Troitzsch and Ellis [21] above 1200°C. Ordered $(Zr,Ti)_2O_4$ is the stable intermediate phase below about 1160°C. Its phase field contrasts that of the disordered form in that it is narrow, spanning only about 2 mol.% at one temperature, but with a distinct dependence on temperature. The average composition of ordered $(Zr,Ti)_2O_4$ changes continuously from $X_{Ti} = 0.649$ at 800°C to 0.604 at 1060°C, where

a jump occurs to about 0.49 at 1080°C. Note that this jump does not correspond to the monoclinic-tetragonal phase transition of the $ZrO_2$ solid solution located between 1080 and 1100°C. Since the abrupt change in $(Zr,Ti)_2O_4$ composition coincides however with a dramatic change in *b*-dimension (Fig. 3) and therefore state of order in the structure, it appears that two distinct ordered phases of $(Zr,Ti)_2O_4$ may have to be distinguished above and below 1070°C. Above this temperature the composition remains unchanged within error to at least 1130°C, but displays another small jump to about $X_{Ti} = 0.515$ at 1160°C, which seems to mark the transition to the disordered phase with b > 5.45 Å (Fig. 3).

A detailed crystal structure study will be necessary to elucidate the processes going on in the transitional phase between 1070 and <1160°C, which displays the dramatic change in *b*-dimension without much variation in composition. This phase was typically found as rims around cores of relic seed composition (Fig. 1d +e). Its crystal shape was rather equi-dimensional (Fig. 1d) and similar to that of the disordered form in our experiments (Fig. 1b), as well as to the disordered $ZrTiO_4$ crystals grown with lithium molybdate flux by Sugai and Hasegawa (1968) [28].

In contrast to this, below 1070°C the ordered phase develops distinctly elongate crystals (Fig. 1a, c). When grown at 800°C with large amounts of lithium molybdate flux (sample ATMU134), ordered $(Zr,Ti)_2O_4$ formed needles up to 0.1 mm long with square cross sections and end-facets (Fig. 1g and h). If optimised, this flux method could provide a way of producing single crystals large enough to be used for dielectric measurements in different crystallographic directions. It could overcome the problems of shrinkage cracks and $ZrO_2$-inclusions in the sintered samples by Azough *et al*. (1986), helping to determine and understand the dielectric properties of this material in comparison to the disordered form [10].

A series of experiments with different compositions at the $ZrO_2$-rich end of the phase diagram (Fig. 2) enabled us to bracket the monoclinic-tetragonal phase transition of Ti-bearing zirconia at 1100°C (runs 10 to 15, Table I). Although tetragonal zirconia is not quenchable, but reverts back to the monoclinic structure upon cooling, its existence in our experiments above about 1090°C is suggested by the higher Ti-content of zirconia at these temperatures (Fig. 2). The six experiments at 1000°C were interpreted as follows. Runs 10 and 12 with starting mixes with 3 and 11 mol.% $TiO_2$ reacted completely to zirconia with $X_{Ti} = 0.03$ and 0.11, respectively, so that run 10 obviously lies within the stability field of the monoclinic phase, and run 12 inside the tetragonal one. Two different zirconia phases coexisted in run 11 (7 mol% $TiO_2$) which were of the compositions $X_{Ti} = 0.098$ and $X_{Ti} = 0.040$. While the Ti-rich phase was well crystallized and formed subhedral to euhedral grains up to 40 $\mu$m in size, the Ti-poor zirconia formed the more finely grained (<5 $\mu$m), interstitial mass (Fig. 1f). We interpret these two zirconias to represent coexisting monoclinic and tetragonal phases at 1100°C, and that run 11 therefore represents the inside of the 'donkey-ear' of the phase transition (Fig. 2). Note that the textures of this sample are distinctly different to those of an incomplete reaction with relic cores of pure $ZrO_2$ described above. Pure $ZrO_2$ was not present in this sample.

Previous studies determined the phase transition temperature of zirconia with heating and cooling experiments that were characterised by strong hysteresis effects and therefore temperature uncertainties. The fluxed method used here entirely equilibrated the zirconia assemblages at the target temperature, allowing a more precise location of the transition temperature or composition. More experiments slightly above and below 1100°C could further detail this area, whereby the different morphologies of the monoclinic and tetragonal populations would help to determine wether a one-phase or a two-phase field was encountered.

## 4. Conclusions

The synthesis method with flux and seeds developed at high pressures [20, 22] was successfully applied to atmospheric pressure syntheses, and effectively equilibrated the phase assemblages in the $ZrO_2$-$TiO_2$ system below 1200°C. The phase diagram thus extended by 400°C, differs from previously published work in that the composition of ordered $(Zr,Ti)_2O_4$ is dependent on temperature, rather than being constant [7, 18]. Moreover, we cannot find evidence for a previously suggested two-phase field of coexisting ordered and disordered $(Zr,Ti)_2O_4$ [7]. Rather, the onset of the ordering transition was marked by the stability of a $(Zr,Ti)_2O_4$ phase with a composition ($X_{Ti} = 0.495$) that differs from both disordered $(Zr,Ti)_2O_4$ above 1160°C and ordered $(Zr,Ti)_2O_4$ below 1060°C. Thus two different ordered phases were distinguished based on their composition. Detailed TEM investigations will be necessary to determine their exact ordering patterns [29].

## Acknowledgements

This work was assisted by the Australian Capital Territory Government with a Proof of Concept Knowledge Fund Grant to both authors and Andrew G. Christy, as well as an ARC grant to David Ellis about Zr-equilibria in the crust and mantle. Discussions with Andrew G. Christy are highly appreciated.

## References

1. F. J. BROWN and P. DUWEZ, *J. Amer. Ceram. Soc.* **37** (1954) 129.
2. L. COUGHANOUR, R. ROTH and V. DEPROSSE, *J. Res. Natl. Bur. Std.* **52** (1954) 37.
3. A. COCCO and G. TORRIANO, *Ann. Chim.* **55** (1965) 153.
4. T. NOGUCHI and M. MIZUNO, *Bull. Chem. Soc. Jpn.* **41** (1968) 2895.
5. A. ONO, *Mineral. J.* **6** (1972) 433.
6. A. SHEVCHENKO, L. LOPATO, I. MAISTER and O. GORBUNOV, *Russ. J. Inorg. Chem.* **25** (1980) 1379.
7. A. MCHALE and R. ROTH, *J. Amer. Ceram. Soc.* **69** (1986) 827.
8. G. WOLFRAM and H. GÖBEL, *Mater. Res. Bull.* **16** (1981) 1455.

9. F. AZOUGH, A. WRIGHT and R. FREER, *J. Solid State Chem.* **108** (1994) 284.
10. F. AZOUGH, R. FREER, C.-L. WANG and G. LORIMER, *J. Mater. Sci.* **31** (1996) 2539.
11. C. WANG, H. LEE, F. AZOUGH and R. FREER, *ibid.* **32** (1997).
12. S. ZHANG, J. LI, J. CAO, H. ZHAI and B. ZHANG, *J. Mater. Sci. Lett.* **20** (2001) 1409.
13. M. BANNISTER and J. BARNES, *J. Amer. Ceram. Soc.* **69** (1986) C269.
14. H. BOYSEN, F. FREY and T. VOGT, *Acta Crystallogr.* **B47** (1991) 881.
15. F. FREY, H. BOYSEN and T. VOGT, *ibid.* **B46** (1990).
16. G. WILSON and F. GLASSER, *Brit. Ceram. Trans. J.* **88** (1989) 69.
17. P. BORDET, A. MCHALE, A. SANTORO and R. ROTH, *J. Solid State Chem.* **64** (1986) 30.
18. E. SHAM, M. ARANDA, E. FARFAN-TORRES, J. GOTTIFREDI, M. MARTÍNEZ-LARA and S. BRUQUE, *ibid.* **139** (1998) 225.
19. A. BIANCO, G. GUSMANO, R. FREER and P. SMITH, *J. Europ. Ceram. Soc.* **19** (1999) 959.
20. U. TROITZSCH, A. G. CHRISTY and D. J. ELLIS, *J. Amer. Ceram. Soc.* **87** (2004) 2058.
21. U. TROITZSCH and D. J. ELLIS, *Europ. J. Mineral.* **16** (2004) 577.
22. U. TROITZSCH, D. J. ELLIS and A. G. CHRISTY Patent Application No. 2003906410 (2003).
23. F. IZUMI and T. IKEDA, *Mater. Sci. For.* **321–324** (2000) 198.
24. A. GADALLA and J. WHITE, *Trans. Brit. Ceram. Soc.* **65** (1966) 383.
25. F.-H. LU, F.-X. FANG and Y.-S. CHEN, *J. Europ. Ceram. Soc.* **21** (2001) 1093.
26. A. MCHALE and R. ROTH, *J. Amer. Ceram. Soc.* **66** (1983) C18.
27. Y. KIM and H. JANG, *J. Appl. Phys.* **89** (2001) 6349.
28. T. SUGAI and S. HASEGAWA, *J. Jpn. Ceram. Assoc.* **76** (1968) 429.
29. R. CHRISTOFFERSEN and P. DAVIES, *J. Amer. Ceram. Soc.* **75** (1992) 563.

*Received 8 November 2004*
*and accepted 22 March 2005*